The Usefulness of the Laplacian in Principal Component Analysis and Dipole Source Localization

Stanley A. Klein* and Thorn Carney*#

Summary: Evoked potentials are difficult to analyze because multiple sources are active simultaneously. Principal component analysis and dipole localization are two techniques that have been used to disentangle overlapping sources. Both of these techniques have problems. Principal component analysis suffers from a rotation ambiguity. Dipole localization suffers from biases when the model used to derive the sources from the scalp potentials is misspecified. Using computer simulations we demonstrate that by applying both of these techniques to the Laplacian of the voltages rather than to the raw voltages the problems associated with the two techniques are reduced. Computer programs for the analyses are presented in an Appendix.

Key words: Laplacian; Dipole; Source localization; Principal component analysis; Misspecification; Evoked potential.

Introduction

The evoked electrical potential (EP) and its magnetic counterpart have great promise as tools for learning about the dynamics of cortical processing. The patterns of activation in the multiple cortical regions responding to different tasks provide important information on cortical organization. A temporal resolution of better than 5 msec is required to follow the temporal sequence of brain activity. This temporal resolution is orders of magnitude faster than the capabilities of PET or functional MRI that depend on changes in blood flow and blood metabolism, but it is well within the capabilities of evoked potentials. The problem with the EP is that the high resistivity of the skull relative to the scalp and brain blurs the electrical potential across the scalp so that multiple sources become overlapped. The challenge is to develop techniques for isolating the multiple overlapped sources. We will focus on electrical potentials but all the issues that we consider also apply directly to evoked magnetic fields.

This paper examines two problems facing researchers who want to use topographic maps of scalp potentials to identify the underlying neural sources. The first problem is the "rotation ambiguity" of principal component analysis (Wood and McCarthy 1984; Mocks 1986). The second problem is the bias in dipole estimation when there are multiple dipoles and the model of the head is misspecified (Zhang and Jewett 1993, 1994a, 1994b; Zhang, Jewett and Goodwill 1994). There is a very simple procedure that lessens the severity of both problems: the use of the Laplacian to sharpers the VEP topography. Before going into the full details we will first describe the two problems.

*School of Optometry, UC Berkeley, Berkeley CA, USA.
#Neurometrics Institute, Oakland, CA, USA.
Accepted for publication: September 18, 1995.
Supported by grant EY04776 from the National Institutes of Health. We would like to thank Amnon Silverstein for his help with icosohedra.
Correspondence and reprint requests should be addressed to Stanley A. Klein, Ph D., School of Optometry, University of California, Berkeley, CA, USA, 94720-2020.

The "Rotation" problem

Suppose we find that the voltage at electrode e, at time t, can be expressed as the sum of two sources or components:

$$V(t,e) = T(t,1)\,E(1,e) + T(t,2)\,E(2,e) \quad (1)$$

The order of the arguments has been chosen so that matrix notation can be used later. The vector E(l,e) gives the voltage distribution across the electrodes for the first source and T(t,l) gives the temporal response of the first source. If we make the linear transformations:

$$E'(1,e) = \cos(\alpha_1)E(1,e) + \sin(\alpha_1)E(2,e) \quad (2a)$$

$$E'(2,e) = \cos(\alpha_2)E(2,e) + \sin(\alpha_2)E(1,e) \quad (2b)$$

and

$$T'(t,1) = (\cos(\alpha_2)T(t,1) - \sin(\alpha_2)T(t,2))/\cos(\alpha_1+\alpha_2) \quad (2c)$$

$$T'(t,2) = (\cos(\alpha_1)T(t,2) - \sin(\alpha_1)T(t,1))/\cos(\alpha_1+\alpha_2) \quad (2d)$$

then it turns out that equation 1 is still valid when written in terms of the transformed components:

$$V(e,t) = T'(t,1)\,E'(1,e) + T'(t,2)\,E'(2,e) \quad (3)$$

for any values of α_1 and α_2. This ambiguity is called the rotation problem because equations 2a - 2d resemble a rotation in two-dimensional space. For the special case of $\alpha_2 = \pi/2 + \alpha_1$ the oblique rotation becomes a rigid (orthogonal) rotation. When the rotation is not rigid (α_2 $\pi/2+\alpha_1$) then the two parameter rotation is called an *oblimax* rotation rather than a *varimax* rotation (Mulaik 1972).

There is a common misconception that multiple sources can be disentangled by taking into account their temporal behavior. Consider for example, the case of two sources. At some times only source 1 is active and at other times only source 2 is active. So it seems reasonable that the two sources could be isolated. The flaw in this argument is that the experimenter doesn't know which are the temporal intervals when only a single source is active. Sometimes an assumption is made that any one source is quiet most of the time. In that case one could do a rotation that minimizes the active period of each source. However, we have no basis for this assumption. It is more likely that there are vast feedback circuits in cortex and that each area has multiple periods of activity.

The present paper, similar to Scherg and von Cramon (1985) and Maier et al. (1987), will not make any assumptions about the time dependence. We will, however, assume that only a limited number of electrodes respond well to a given source. The goal then is to find the values of α_1 and α_2 in equation 2 that makes the functions E'^e) and $E'_2(e)$ as localized as possible (in electrode space) as would be expected of a localized source. This goal can be met by maximizing the "varimax" or "oblimax" quantity:

$$M(\alpha_1) = \Sigma\, E'(1,e)^4 \,/\, (\Sigma\, E'(1,e)^2)^2 \quad (4)$$

It is helpful to consider a simple example with two electrodes, E(i,l) and E(i,2), to see why maximizing M is a good thing. Suppose E(l,e) = (.8, .6) and E(2,e) = (-.6, .8). Before any rotation the varimax magnitude is M(0) = ($.8^4$+ $.6^4$)=.5392. If tan (α_1) is chosen to be -.75 then E'(l,e) = (1,0) and M(-.75) = 1. This value of M (unity) is the maximum possible. Since we are assuming that the true underlying sources produce the narrowest possible electrode distributions we see that the varimax rotation has succeeded in finding the correct solution since the distribution (1, 0) is the narrowest possible one.

There is an obvious problem with this procedure. It might well be that the *true* sources are not narrow and the oblimax rotation produces sources that are artificially narrower than the true sources (Wood and McCarthy 1985; Mocks and Verleger 1986). In this paper we show that it is advantageous to use the Laplacian of the electrode distribution rather than the raw electrode distribution as has been done by all previous authors for the oblimax rotation. We will show that the Laplacian distribution is narrower than the original distribution so that the oblimax rotation will do a better job of rotating to the true sources. The Methods section will go through all the derivations for the general case.

The misspecification problem

For the misspecification problem we take as our starting point the topography of electrode voltages at one instant of time. We are interested in predicting the set of underlying dipole sources from this scalp voltage. This is called the inverse problem. The reason for going to dipole sources is that we are interested in knowing the approximate location of the activity in the brain. By misspecification we mean that an incorrect formula is used to represent the voltages due to a single dipole. The misspecification occurs because the formula that is typically used for the inverse problem is the formula for a dipole in a spherical, one-shell head. The true head is not spherical and it has more than one shell (the skull and scalp make the true situation at least a 3-shell problem). Ary, Klein and Fender (1981) showed how a correction term could be developed for a single dipole in a 3-shell spherical head that is fit by a 1-shell dipole. They used a least squares procedure to find the best fitting 1-shell dipole. The model is not perfect so there is a residual error due to the misspecification. If more than one dipole is present the residual voltage from the misspecified fit from one dipole will perturb the locations and magnitudes of the other dipoles (Zhang and Jewett 1993, 1994a, 1994b; Zhang, Jewett and Goodwill 1994). In this paper we will consider the misspecification caused by a nonspherical head and will show there are circumstances where the biasing effect can be large. We will also show that if the source localization algorithm is applied to the Laplacian rather than to the original data, the bias produced by misspecification is reduced. This is because the Laplacian greatly reduces the effect of the far field. It is the far field that suffers the greatest amount of misspecification due to head nonsphericity, so reducing its effect reduces the bias.

Methods

Electrodes

A 7 x 7 square array of 49 electrodes were used in all the simulations. We wanted a square array to simplify

the Laplacian calculation. As discussed by Klein (1993) it is possible to take the Laplacian of non-regular electrode arrays, but for present purposes we opted for the simpler, regular case. It is a challenge to space electrodes evenly on a spherical surface. We have chosen to place the electrodes uniformly in θ and φ with values of θ and φ going from -45 deg to +45 deg in seven 15 deg steps. Since 15 deg corresponds to about .26 radians, it corresponds to 2.6 cm for a 10 cm radius skull. The Cartesian x and y values are chosen to be:

$$x = \sin(\varphi)\cos(\theta/2) \quad (8)$$

and

$$y = \sin(\theta)\cos(\varphi/2) \quad (9)$$

the position along the z-axis is given by:

$$z = (1-x^2-y^2)^{.5} \quad (10)$$

Thus, for example, the corner electrode at θ = φ = 45 deg has coordinates of (x, y, z) = (.65, .65, .38). The particular choice of coordinates is halfway between treating the x and y coordinates as major circles (longitudes) and minor circles (latitudes). It enables the x and y coordinates to be symmetric and close to orthogonal. The angular spacing, α, between neighboring electrodes can be calculated by taking the dot product between the two locations:

$$\cos(\alpha) = x_1x_2 + y_1y_2 + z_1z_2 \quad (11)$$

Along the meridian, θ = 0, the three separations of the four electrodes from φ = 0 to 45 deg are all 15 deg. For θ = 15 the three separations are 14.9, 14.9 and 15.0 deg. For θ = 30 deg the separations are 14.5, 14.6 and 14.9 deg. Finally for θ = 45 deg, the separations are 13.9, 14.2 and 15.3 deg. All other separations are given by symmetry. Since all separations are fairly close to 15 deg we approximated the Laplacian (see the Appendix for the program that was used for calculating the Laplacian) by assuming that all separations were equal. Small errors are being made near the corner electrodes.

The one-shell model for a spherical head

Fortunately for dipole source localization there is a relatively simple closed form formula for the scalp potential due to a dipole in a one-shell spherical head (Brody 1973). If a dipole with magnitude M, is located at position r, then the voltage at an electrode at position E is given by:

$$V(E,r,M) = M\,F(E,r) \quad (12)$$

with

$$F(E_j r) = [E + 2(E-r)/d^2 + (E\,(E\,r) - r)/(d+1-E\,r)]/d \quad (13)$$

and where d is the distance between the electrode and dipole, d = I r - EI and $E^2 = 1$ since the electrodes are on a unit sphere. Note that all quantities in bold type are three-dimensional vectors. The nonlinear function F specifies how the electrode Voltage depends on dipole location. In the source localization problem we are given V and must find M and r. Equation 12 shows that the voltage is linearly related to the magnitude, so the determination of M can be done simply by using linear regression once one knows F(E,r) and the voltages on the electrodes. The determination of r involves nonlinear regression for which we use the Marquardt-Levenberg algorithm (see Press et al. 1986 for a description). Our *Brodyinv* function, (see Appendix) demonstrates, for the case of two dipoles, how one can combine a nonlinear regression for r together with a linear regression for M.

Choice of dipoles for simulations

For both the "component rotation" simulation and the "misspecification" simulation two dipoles will be used. A totally general dipole is specified by 6 parameters, 3 values for M and 3 for r. In our simulations we will, for simplicity, reduce the number of parameters in the forward solution by taking the original dipoles to lie in the x, z plane (y=0). The dipoles used in the inverse solution are allowed to move away from y = 0. As a reminder, the central electrode is at the top of the head, on the z axis, and is specified by θ = φ = x = y = 0.

In most of the simulations one of the dipoles will have its position and its orientation on the z-axis ($x_\tau = y\backslash = M_{1x} = M_{1v} = 0$).- The position and orientation of the second dipole is varied. Since the first dipole is aligned with the z-axis, the coordinate system can be rotated so that the second dipole lies in the x - z plane ($y_2 = 0$) without any loss in generality. For this group of simulations, the magnitude of the second dipole is chosen to equal that of the first dipole. Further details are given in the Results and in the Appendix where the computer program that carried out these simulations is presented and discussed.

In some of our simulations the pair of dipoles will be mirror images specified by a total of three parameters: the location (x, z) and orientation (γ) of one dipole. The location and orientation of the other dipole will be reflected about the z-axis in the y = 0 plane:

$$z_2 - z_1,\ x_2 = -x_1,\ y_2 - y_1 = 0 \quad (14)$$

$$\tan(\gamma) = M_{2x}/M_{2z} = -M_{1x}/M_{1z},\ M_{1y} = M_{2y} = 0 \quad (15)$$

In order to gain an understanding of the effect of the dipole magnitude, in this simulation the right-hand dipole is chosen to have twice the strength of the left-hand dipole.

The Laplacian

There has been some controversy about whether the Laplacian provides a measure of the density of current sources (Srebro 1992; van Dijk and Spekreijse 1992). That controversy is not relevant to the present enterprise since our only interest is that the Laplacian removes slowly varying components of the voltages. The reader should be warned that the title of the van Dijk and Spekreijse paper: "The 2 dim-Laplacian field is not suitable to localize sources of EEC activity" does not imply that the Laplacian is not useful for dipole source localization. The point of the van Dijk and Spekreijse paper is that the raw Laplacian topography may not be directly interpretable as a current source density distribution. Consider, for example, a purely tangential eccentric source. The scalp topography as well as the Laplacian will have two peaks (one positive and one negative) that are shifted away from the location of the underlying source. We do expect, however, that the Laplacian will always give a better picture of the underlying sources and the underlying cortex potential than the original scalp potential. The advantages of the Laplacian in the context of surface topography are discussed in greater detail by Nunez and Westdorp (1994). A full solution of the inverse dipole localization problem is needed to obtain a more accurate picture of source locations. That is the topic of our Problem #2.

All of the simulations to be described will be done twice, first with the original voltages at each electrode and then with the Laplacian of the voltages. In the limit of very close electrode spacing the Laplacian is proportional to the second derivative of the voltages at the electrodes. In our case of finite electrode spacing the Laplacian can be approximated by taking a balanced difference of the voltage at one electrode and the voltages of the surrounding electrodes. There are three arrangements of electrodes relevant to taking the Laplacian for our square array of 49 electrodes: corner, edge and inner. For the 25 inner electrodes the Laplacian is given by:

$$L(\theta,\phi) = V(\theta,\phi) - \tfrac{1}{4}(V(\theta+15°,\phi) + V(\theta-15°,\phi) + V(\theta,\phi+15°) + V(\theta,\phi-15°)) \quad (16)$$

For the 10 upper and lower edge electrodes the Laplacian is:

$$L(\theta,\varphi) = V(\theta,\varphi) - \tfrac{1}{2}(V(\theta,\varphi+15°) + V(\theta,\varphi-15°)) \quad (17)$$

For the 10 right and left electrodes it is:

$$L(\theta,\varphi) = V(\theta,\varphi) - \tfrac{1}{2}(V(\theta+15°,\varphi) + V(\theta-15°,\varphi)) \quad (18)$$

Finally the Laplacian at the four corner electrodes are ignored in our algorithms by setting the corner "Laplacian" voltage to zero.

Law, Nunez and Wijesinghe (1993) develop a spline Laplacian formalism whereby if one has full information about the head shape and conductivities of the various head components then one *tan* improve the estimate of the Laplacian over the first order approximation given in equations 16 - 18. The advantages of the spline Laplacian are discussed further by Nunez and Westdorp (1994).

Now that we have the locations of the electrodes and the formula for the potential due to a dipole, we are ready to proceed with the two problems discussed in the Introduction.

Problem #1: Principal Component Analysis and the "rotation" ambiguity

Decomposition into sources and the oblimax rotation

The goal of this section is to show why the Laplacian reduces the rotation ambiguity in the principal components approach to finding the underlying sources of the evoked potential. Before getting to the role of the Laplacian we will first develop the fqrmalism for the oblimax rotation. The raw data is V(t,e) where there are N_e electrodes indexed by *e,* and N_t time intervals indexed by *t.* It is a general theorem from linear algebra (Press et al. 1986) that any matrix can be decomposed as follows, using a singular value decomposition (SVD):

$$V(t,e) = \sum_{i=1}^{N_m} T_o(t,i)\, w(i)\, E_o(i,e) \quad (19)$$

where the matrices T_0 and E_0 and the vector w, are the output of the SVD algorithm. The summation over i goes from 1 to N_m where N_m is the minimum of N_e or N_t. The weightings w(i) are positive numbers arranged in decreasing order so that w(i+l) w(i). The subscript *o* means the different components are orthonormal to each other:

$$\sum_{t=1}^{N_t} T_0(t,i)T_0(t,i') = \sum_{e=1}^{N_e} E_0(i,e)\, E_0(i',e) - \delta_{ir} \quad (20)$$

The Kronecker delta function is unity if i=i' and is zero otherwise.

Principal component analysis involves truncating the summation of equation 19 to N_s terms rather than the full N_m terms. The mean square error produced by this

truncation is:

$$R(N_s) = \sum_{t=1}^{N_t}\sum_{e=1}^{N_e}(V(t,e)-V_{trunc}(t,e))^2 = \sum_{i=N_s+1}^{N_m} w(i)^2 \quad (21)$$

where V_{trunc} is the truncated matrix of voltages. The total sum of squares of all the voltages is obtained by setting V_{trunc} equal to zero so that the right hand side of equation 21 is the sum of squares of all the w(i) values. The basic assumption of advocates of principal component analysis is that by keeping the first few principal components, the residual square error is relatively small:

$$R(N_s)/R(0) \ll 1 \quad (22)$$

This is a reasonable assumption because investigators (Darcy, Ary and Fender 1980; Meier et al. 1987) have shown that the evoked potential is dominated by a small number of principal components. Maier, for example, finds that at least 93% of the variance in the voltages at 24 electrodes can be accounted for with just two principal components for the time interval between 71 and 171 msec after pattern onset. Kavanagh, Darcy and Fender (1976) found that 5 sources are needed to account for 95% of the variance up to 250 msec.

The usefulness of the SVD decomposition can be understood by counting parameters. The raw data involved N_eN_t values. In our case N_e = 49 and N_t is typically 100 (3 msec sampling and a 300 msec record). Thus there are 4,900 data points. If the w(i) values indicate that two components account for most of the response then there would be 48, 47, 99, 98 and 2 parameters for E(l,e), E(2,e), T(t,l), T(t,2) and w(i) respectively for a total of 294 parameters. This is a 16-fold reduction in the number of parameters needed to specify the data.

Following the SVD decomposition we perform a "rotation". The rotation can be clarified by first rewriting equation 19 in matrix notation.

$$V = T_0 W E_0 \quad (23)$$

where W is a diagonal matrix with elements w(i). In equation 23 we are limiting the range of i to go only over the N_s principal components that are large. The rotation is achieved by inserting a rotation matrix, R, and its inverse in equation 23:

$$V = T_0 W R^{-1} R E_0 \quad (24)$$

$$= TE \quad (25)$$

where

$$E = R E_0 \text{ and } T = T_0 W R^{-1} \quad (26)$$

This is a generalized version of what we showed in equations 2 and 3. Equations 25 and 26 group the magnitude elements w(i) together with the temporal factors T. Since the true underlying sources that we seek may not be orthogonal, the rotation of components must be more general than a rigid rotation. For a rigid rotation all the rows are orthonormal and likewise for the columns. This leads to $N_S(N_S - 1)/2$ parameters for a rotation in N_s dimensional space. For the general nonorthogonal case (oblique rotation) there are N_S^2-N_S parameters (twice as many as for a rigid rotation). The term N_s is subtracted off because each row of R is normalized to unity. For N_s=2 (the case discussed in the Introduction, equations 1 - 3) the oblique rotation can be written as:

$$R = \begin{bmatrix} \cos(\theta_1) & \sin(\theta_1) \\ \cos(\theta_2) & \sin(\theta_1) \end{bmatrix} \quad (27)$$

This oblique rotation would be a rigid rotation (maintaining angles) if $0_2 = \pi/2 + QI$. For $N_s = 3$ the oblique rotation can be written as:

$$R = \begin{bmatrix} \cos(\theta_1) & \sin(\theta_1)\cos(\varphi_1) & \sin(\theta_1)\sin(\varphi_1) \\ \cos(\theta_2) & \sin(\theta_2)\cos(\varphi_2) & \sin(\theta_2)\sin(\varphi_2) \\ \cos(\theta_3) & \sin(\theta_3)\cos(\varphi_3) & \sin(\theta_3)\sin(\varphi_3) \end{bmatrix} \quad (28)$$

As was discussed earlier, the purpose of the rotation is to produce a topography map that is most concentrated, with the hope that the concentrated topography is similar to that produced by the true underlying sources. An oblique rotation with the maximization criterion given by equation 4 will be called a oblimax rotation condition (Mulaik 1972).

A good test of the oblimax rotation involves the following simulations, following the strategy outlined by Wood and McCarthy (1984) in their critique of principal component analysis.

1) Start with known sources, with known electrode distributions E(i, e) and known temporal responses T(t, i). The matrices E and T are underlined to indicate that these are the true distributions. The E matrix is calculated in our simulations by positioning two or more dipoles in the head and using the Brody formula (equation 12) to calculate the voltages on the electrodes (and then normalizing to unity Pythagorean sum). The T matrix is arbitrary, with the condition that there must be at least as many time intervals as there are dipole sources.

2) Calculate the voltage matrix:

$$V = V(t,e) = \sum_{i=1}^{N_S} \underline{T}(t,i)\underline{E}(i,e) \quad (29)$$

3) Do a singular value decomposition of the V matrix as in equation 19, resulting in matrices E_0, W, and T_0. These are the unrotated, orthogonal components that need not be similar to the true underlying sources.

4) Do an oblimax rotation as in equation 26 resulting in matrices E' and T'.

5) Compare the resulting matrices E' and T' with the initial matrices E' and T'.

The above 5 steps are similar to the procedure carried out by Wood and McCarthy (1984) except for two features: 1) Wood and McCarthy use a rigid rotation (varimax) rather than a more general oblique transformation (oblimax). We believe the latter is appropriate since the underlying components need not be orthogonal. 2) They apply the rotation to the time matrix, T, whereas we apply it to the electrode weightings, E. We believe that there is no convincing evidence that the temporal response of a single source has a narrowly peaked structure. Scherg and von Cramon (1985) and Maier et al (1987) provide supporting evidence for this belief. Therefore it would be inappropriate to apply the oblimax condition to the temporal waveform. The electrode distribution from an eccentric dipole, on the other hand, will produce a tight response across electrodes. Wood and McCarthy (1984) found that if one started out with principal components that had a strong overlap (not narrowly tuned) then the varimax rotation produced final factors that were more narrowly tuned. Thus the rotated factors did not agree with the original factors. The message is that one should work with situations where the underlying factors are narrowly tuned. That is the reason that we are investigating whether the Laplacian goes in this direction.

Mocks and Verlager (1986) offered a simplification of the Wood and McCarthy simulations. They pointed out that the end result of the varimax rotation did not depend on the starting point. So rather than starting from the output of the SVD calculation (E_0 in our case) they started from the original true components (E in our case). They bypassed steps 2 and 3 of the 5 steps outlined above by not introducing any temporal dependence. To demonstrate that their procedure is equivalent to that of Wood and McCarthy they point out that their final rotated components were identical to those found by Wood and McCarthy. We will follow the path of Mocks and Verlager.

Results

The simulations

To keep things simple we will restrict our simulations to two dipoles. Two dipoles are specified by 12 parameters, which is much too large a space to explore and to conveniently display the results so some of the coordinates are constrained as discussed earlier in the section titled "Choice of dipoles for simulations".

The oblimax function M(α) given by equation 4 is plotted for the case where there is some overlap. Two examples will be shown. The dipole parameters for the first example (figure la, left panel) are taken to be mirror symmetric at a 'latitude' of 45 deg and an eccentricity of .7:

$$-I_t=(x_t,y_t,Z_tH-\ 7/V2,\ 0,\ .7/V2) \quad £=(.7/\hat{}2,\ 0,\ .7A/2) \quad (30a)$$

$$Mi = (M_{lx},M_{ly},M_{lz}) = (0,0,1) \quad M2=(0,0,l) \quad (30b)$$

For the second example (figure Ib) the only change is that the location of the first dipole is taken to lie on the z axis, while its eccentricity is the same as before (equation 30a): ft = (0,0, .7).

The Brody formula given by equations 12 and 13 is then used to calculate E(l,e) and'E(2,e) for the two dipoles. One of the rotated electrode weightings can be calculated according to equation 27:

$$E'(l, e) = \cos(\alpha)\ E(l, e) + \sin(\alpha)\ E(2, e) \quad (31)$$

Equation 31 is then plugged into the oblimax maximization function given by equation 4:

$$M(\alpha) = \sum_{e=1}^{N_e} E'(1,e)^4 \,/\, (\sum_{e=1}^{N_e} E'(1,e)^2)^2 \quad (32)$$

The function M(α) for the two dipole sources given by equation 30 is plotted in figure la as the solid line. It is seen that the function has two maxima, near $\alpha = (1-.136)\pi = 2.71$ and $\alpha = (.5+.136)\pi = 2.00$. It is gratifying that there are two maxima because we need two solutions, one for each of the original components. The two original components correspond to $\alpha = 0$ and $\alpha = \pi/2$. For mirror image dipoles of our first example, the two maxima will always be symmetrically placed around the minima at $\alpha = .75\pi$ or $.25\pi$. In addition, the maxima repeat whenever α is incremented by π, so there is a maximum near zero, at $\alpha = -.136\pi = -.43$. As can be seen in equation 31, the solution near $\alpha = 0$ is close to the original component E(l, e) and the solution near $\alpha = 90$ deg is close to E(2, e).

The choice of dipoles specified by equation 30 corresponds to a case where the oblimax rotation as applied to

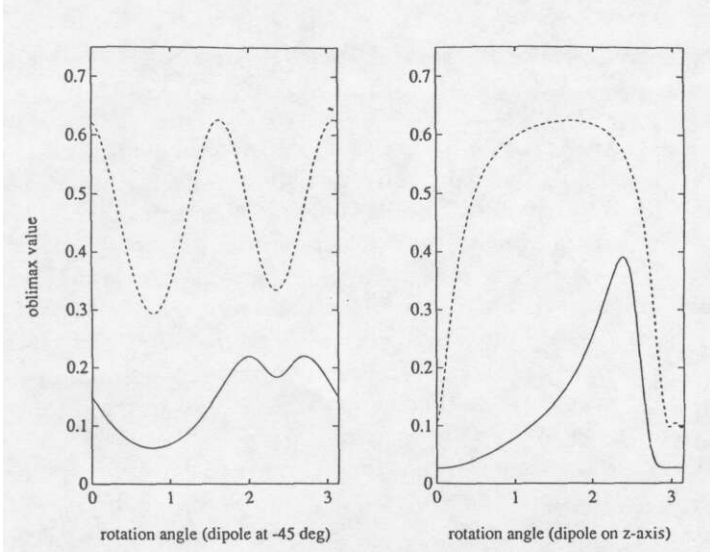

Figure 1. The quartic oblimax function given by equation 32 plotted as a function of the rotation angle alpha (α). The dotted line is the Laplacian case, solid line is non-Laplacian. The left panel (a) is for the symmetric pair of dipoles specified by equation 30, at an eccentricity of 0.7 and a 'latitude' of 45 deg. For the right panel (b) one of the dipoles is shifted to be on the z-axis and its eccentricity is still at 0.7. The orientation of both dipoles is in the z-direction and they have equal magnitudes. Note that each curve has two maxima (including the lower curve of the right panel). In the right panel the maximum near α=π is very weak and easily missed by standard maximization routines. The feature of these plots of interest to us is the location of the maxima. It is seen that with the Laplacian the maxima are closer to the 'true' sources at a=π/2 and 0 (or π due to the repeating nature of the oblimax function). The fact that the oblimax function is larger in the case of the Laplacian means that the electrode distribution has sharper peaks, as discussed in the text.

the SVD decomposition introduces a small bias (~.136π radians) since the rotated solutions are not identical to the correct original solution. We also explored cases in which one of the dipoles had a larger magnitude than the other. We found that the stronger dipole was associated with the larger rotation. At first we were surprised since we expected the stronger dipole to be more resistant to being perturbed, but then we realized that the stronger dipole could tolerate a larger rotation since the rotation adds a weak extra component. Thus a stronger dipole is less sensitive to rotations.

One can write an equation for the location of the maxima and minima of equation 32 by setting the derivative of M(α) equal to zero. As shown by Mulaik (1972) this leads to a fourth-order equation. A fourth-order equation can have four real roots in which case the function M will have two maxima and two minima. That is the situation shown in figure la. As the two dipoles get closer together, thereby increasing the overlap, two of the roots become imaginary and only one maximum is obtained. In this case the oblimax rotation will fail to give anything useful. The two curves shown in figure 1b are near this transition, though both still have two maxima. It is interesting to speculate what happens to the oblimax function in the case of more than two dipoles. In the case of 3 dipoles, equation 31 becomes a function of two angles, αl and α2, rather than just α, and we would expect that in the al, a2 plane three maxima would be found corresponding to the three principal components.

The dotted lines in the two panels of figure 1 are for the case in which a Laplacian of the electrode voltages is taken before M(α) is calculated. The two underlying dipoles are the same as for the solid line. The Laplacian reduces the rotation angle to α= (1-.015) π= 3.09 and α= (.5 + .015)π = 1.62 for the two peaks in figure la. This is almost a ten-fold reduction in the rotation angle bias. This reduction in the oblimax rotation angle bias is the basis for our argument of why the Laplacian is useful in principal component analyses.

Whereas for the solid line all 49 electrodes were included, for the Laplacian the four corner electrodes did not contribute. We also calculated M(α) for the non-Laplacian case with 45 electrodes and M(α) was not significantly different from the 49 electrode case.

The oblimax function for the case when the location of one of the dipoles is shifted to the z axis is shown in figure 1b. The function looks quite different from the symmetric dipoles shown in figure la. Even though the functions look very different the locations of the maxima are fairly similar. For the non-Laplacian case the maxima are at: α= (1 - 0.035) π= 3.03 and α= (0.5 + .258) π= 2.38. With the Laplacian the maxima are at: α= (1 - 0.035) π= 3.03 and α=(.5 + .046) π= 1.72. For this dipole configuration the Laplacian doesn't affect the rotation angle for the first dipole (the one on the z axis) but it reduces the error of the angle for the second dipole from .258π to .046π .

One cautionary remark is needed for finding the maxima of the function M(α). Since there are usually two maxima there is a strong possibility that the "wrong" maximum will be found. Note in figure 1b that the maximum near 0 or π is very weak. If one isn't very careful the maximization routine will miss the maximum near zero and find the global maximum instead. To avoid this possibility we always started our search at α= 0 with a small step size of α= .04. We wrote our own maximization routine for finding the local maximum and avoid getting trapped in the global maximum! This is especially important for asymmetric sources when the two maxima have unequal heights as in figure 1b. Details of this algorithm are presented in the Appendix (Function #2, *oblimax)* which contains the computer programs that were used.

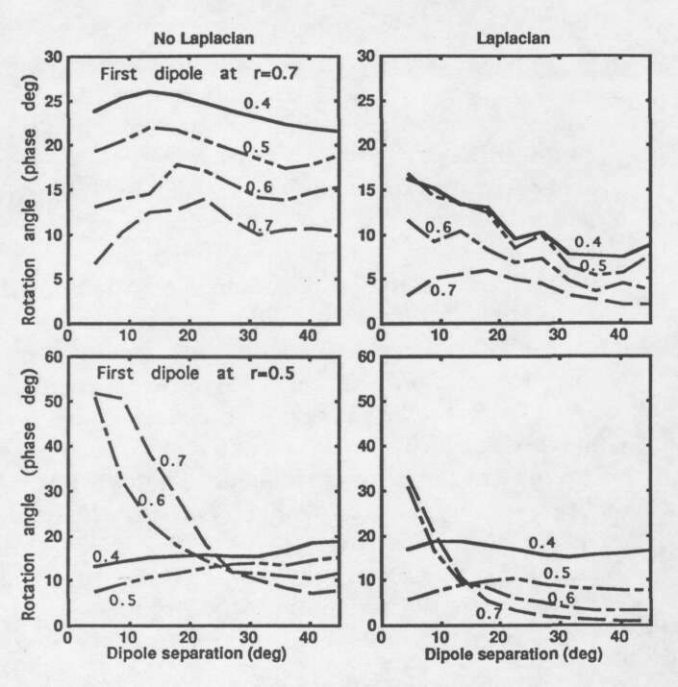

Figure 2. Simulations of the bias in the oblimax rotation. Top panels: the first dipole is a radial dipole fixed on the z axis at an eccentricity of 0.7. Bottom: it is fixed at an eccentricity of 0.5. Ordinate = median rotation angle bias in a set of calculations in which the orientation of the second dipole was directed in 42 directions uniformly distributed over a sphere. The 4 curves in each panel represent 4 radii of the second dipole: 0.7, 0.6, 0.5 and 0.4. Abscissa = angular separation between the dipoles. The left and right panels = non-Laplacian and Laplacian cases, resp. When one dipole has an eccentricity of >0.5 and the dipoles are separated by >15 deg, the oblimax rotation angle for the Laplacian case is about <10 deg, a reasonably small value. Without the Laplacian it is unacceptably large.

In both examples of figure 1 the Laplacian has the advantage of producing a smaller bias. That is, given the original data V(t,e), the procedure of singular value decomposition followed by the oblimax rotation gives a solution very close to the correct sources if the Laplacian is used but would introduce a significant bias if the original voltages were used.

Simulations were done in order to provide a quantitative estimate of the error alpha, in the oblimax rotation angle for a range of dipole locations and orientations. The top panels of figure 2 show the results for the case where the first dipole was fixed on the z axis at an eccentricity of .7. Its orientation was also fixed to be along the z axis, so that it was a radial dipole. The bottom two panels are for the first dipole fixed at an eccentricity of .5. Since the first dipole was a radial dipole on the z axis, the second dipole could be chosen to lie in the x-z plane without any loss of generality. Figure 2 shows plots of the oblimax rotation angle α, on the ordinate vs. the angular separation of the two dipoles on the abscissa. The separation, specified as the angular distance of the second dipole from the z axis, varies from 4.5 to 45 deg in ten steps. Precise details of this calculation are presented in the Appendix in the form of computer programs. The four curves in each panel of figure 2 correspond to the four eccentricities of the second dipole: either .7, .6, .5 or .4 as indicated in the Figure. The magnitudes of the two dipoles are equal. The curves represent the median angle over 42 three-dimensional orientations of the second dipole, uniformly spread over a sphere. Uniform coverage was achieved by starting with the 12 vertices of an icosohedron. An additional 30 vertices were obtained by bisecting each edge of the icosohedron and then projecting that midpoint onto the unit sphere. The resulting 42 vertices are the same as used in many geodesic dome designs. The computer code for generating the 42 vertices is found in the Appendix (Function #6, *vert*42*)*.

The left-hand panels of figures 2 are for the non-Laplacian case and the right-hand panels are for when the Laplacian of the voltages is taken. It is seen that in most cases, use of the Laplacian reduces the error in the oblimax rotation by about 50%. Ideally the rotation angle alpha, plotted on the ordinate, would be zero since in that case one would end up with the original sources. Note that the smallest rotation angle is usually found when the two dipoles have the same eccentricity. With the Laplacian there is a wide range of rotation angles for which the error is below 10 deg. This analysis shows that for a pair of eccentric dipoles, a singular value decomposition followed by an oblimax rotation may be justified for the two dipole situation when a Laplacian is taken. Without the Laplacian the rotation angle is almost always greater than 10 deg and therefore the solutions obtained from principal component analysis are not trustworthy as representing the original sources.

Problem #2: Biases in source localization due to misspecified models

It is very common in dipole source localization to use the Brody formula (Brody et al. 1973) for a dipole in a 1-shell homogeneous head. This analytic formula is used to speed up the calculations needed to solve the inverse problem (the case where the potential is given and one must find the best fitting dipole). A least squares search is needed in which the dipole formula must be recalculated hundreds of times in order to converge to the optimal fit while avoiding local minima. If one went beyond the Brody formula to methods that allow for more than one shell, for changing skull and scalp thickness, and for non-spherical heads, the process of finding the optimal

solution would take too much time. As was discussed in the Introduction, a bias is introduced when one uses the simplified model. Ary, Klein and Fender (1981) calculated the bias for a single dipole given a three-shell forward solution and a one shell (Brody formula) inverse solution. In order to obtain an analytic solution the head was considered to be covered with electrodes continuously over the full 4π steradians of the sphere, enabling analytic integration over the sphere. The Ary correction for a single dipole has been verified (Jewett, personal communication) when a more realistic array of electrodes is used.

As pointed out by Zhang and Jewett (1993, 1994a, 1994b) and Zhang, Jewett and Goodwill 1994) an insidious problem arises when a second dipole is introduced since the residue of the misspecified fit of the second dipole will affect the fit of the first dipole. As discussed in the Introduction we believe that by using the Laplacian the interactions due to multiple dipoles will be reduced. This is because, at least for our simulations using non-spherical heads, the misspecification is most severe in the far field. Locally the head can be approximated by a sphere but far away it deviates strongly from a sphere. In this paper we examine one extreme version of a non-spherical head: a half-sphere.

The half-sphere model

The head shape that we will examine is a half-sphere with uniform conductivity. For $z>0$ the region of uniform conductivity is bounded by a surface of zero conductivity at unity radius (the scalp). In addition there is a plane of zero conductivity at $z=0$. This plane of zero conductivity is what makes our head different from any previously explored. If one looks at pictures of the bone structure surrounding human brains one see that it indeed looks more like a half-sphere than a full sphere. In any case the realism of our head shape isn't important. We just want to use a non-spherical head shape for which we can find the forward solution and then use the Brody solution for a spherical head for the inverse problem. We want to look at the biases produced by this misspecification and examine whether the biases are reduced by using the Laplacian.

The formula for the potentials on the surface of a half-sphere are easy to obtain by using the method of images that is so familiar to physics students in their electricity and magnetism course. The formula for the voltage, V_h, at electrode position E on a half-sphere due to a single dipole can be calculated by adding an image dipole that is reflected in the $z=0$ plane. That is:

$$V_h(E, r, M) = V(E, r, M) + V(E, r', M') \qquad (33).$$

where V(E, r, M) is the Brody formula (equation 12) for a dipole at r with magnitude M and

$$r = (x, y, z), \qquad r' = (x, y, -z)$$

$$\text{and } M = (M_x, M_y, M_z), \quad M' = (M_x, M_y, -M_z) \qquad (34)$$

That is, the potential on the upper hemisphere due to a single dipole in a half-sphere is equal to the potential on that hemisphere due to the dipole and its image in a full sphere. For an image solution to work two conditions have to be satisfied: 1) the charge distribution within the boundary has to be the same in the two situations. 2) the boundary conditions have to be correct in both situations. The first condition is satisfied since in both the original half-sphere situation and in the full-sphere plus image situation there is the same single dipole in the upper half of the sphere. The second condition imposes the following boundary condition on the two situations. No current must leave the hemisphere at a radius of 1 for $z>0$, and no current must pass through the plane at $z=0$. In the half-sphere case the boundary condition is satisfied because the conductivity is zero outside the half-sphere so currents can not exit. In the full-sphere plus image situation the boundary condition on the hemisphere is satisfied because the Brody formula is used. This formula was derived specifically to enforce the spherical boundary conditions. The second boundary condition that no current passes through the plane $z=0$ is enforced by symmetry by our choice of a mirror-reflected image dipole. This model for a non-spherical head is convenient to use because there is an analytic formula specifying the voltages on the scalp.

Linear regression for magnitudes

The computation can be time consuming. The simulations that went into figures 5 and 6 involved 6,720 double dipole source localizations (2 eccentricities for the first dipole, 4 eccentricities for the second dipole, 42 orientations for the magnitude of the second dipole, 10 'latitudes' for the second dipole, presence and absence of the Laplacian). Our long-range goal is to do source localizations with real data using many electrodes, with many simultaneously measured stimulus locations and with many dipoles at a time. In order to optimize the speed and the robustness of the nonlinear regression for these large calculations the search algorithm should be efficient. A two dipole problem involves a 12 parameter least squares fit. It is always advantageous to reduce the number of parameters in the nonlinear search. Equation 12 shows that the magnitude parameters enter linearly, so the least squares search can be split into a nonlinear search for the dipole locations and a linear regression for

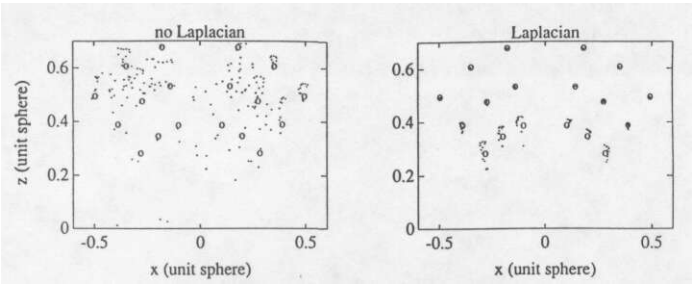

Figure 3. Errors in dipole localization when the volume conduction model is misspecified. The misspecification was produced by basing the forward solution on a "half-sphere" and the inverse solution on a full sphere. Nine pairs of symmetrically placed dipoles are used. Right panel = Laplacian; left panel = non-Laplacian. The abscissa and ordinate are the x and z coordinates of locations in the y=0 plane of unit sphere. Locations of original dipoles indicated by the open circles. Dots indicate locations of dipoles found by nonlinear regression least square search. When the Laplacian was used, these were localized close to the original dipoles. Without the Laplacian the mislocalization is severe. Right side dipoles had twice the strength of left side dipoles. As expected, the displacement of the weaker dipole was larger than that of the stronger dipole.

their magnitudes (Maier et al. 1987).

Here we would like to point out how elegantly Matlab does the linear regression. For a two dipole fit Equation 12 can be rewritten as:

$$V_E(r, M) = M_r F_{1E}(r_1) + M_2 F_{2E}(r_2) \quad (35)$$

$$= M F_E \quad (36)$$

where M is a 6 dimensional vector (the magnitudes of the two dipoles) and F_E is a 6 x N_e dimensional matrix where N_e is the number of electrodes. The linear regression is done just after F_E is calculated based on the present values of the dipole locations τ_r. The Matlab instruction for the linear regression is simple (see Line 9 of the *Brodyinv* function in the Appendix):

$$M = data_E \quad F_E \quad (37)$$

where $data_E$ are the voltages on the N_e electrodes (a 1 by N_e vector) obtained either from a real experiment or from the misspecified forward solution in our simulations. Division by a non symmetric matrix is called a "pseudo-inverse" and what is actually going on in equation 37 is:

$$M = \left(\sum_{e=1}^{N_e} data_E F_E\right) * \left(\sum_{e=1}^{N_e} F_E F_E\right)^{-1} \quad (38)$$

where the summation is over all the electrodes. The quantity $\sum_{e=1}^{N_e} F_E F_E$ *is a 6x6* matrix that gets inverted by standard matrix inversion. Equation 38 is a standard way to do linear regression. The Matlab convention in equation 37 is not only more elegant it also allows for a more efficient, faster calculation.

Stimulations

The first set of simulations used a pair of dipoles symmetrically placed in the x-z plane. The locations of the two dipoles were mirror imaged around the x-axis, so the two dipoles have locations of (x, z) = (-r sinλ , r cosλ) and (r sinλ , r cosλ). The eccentricities were r = .4 , .55 and .7.. The "latitudes" of the sources in the y=0 plane were λ=±15, ±30 and ±45 degrees. The dipole orientations, constrained to the x-z plane, were incremented by 15 deg, making a total of 12 orientations. Only 180 degrees of orientations (not 360 degrees) need to be explored because of the symmetry of the problem. The orientation of the second dipole was mirror imaged around the plane x = 0. The right-hand dipole has twice the strength of its partner so their magnitudes are (M_x, M_z) = (-sinθ, cosθ) and (2sinθ, 2cosθ), where θ is the direction in which the dipole is pointing.

Figures 3a and b show the results of these simulations without and with the Laplacian respectively. The circles show the original locations of nine dipole pairs in a unit sphere. Each dot gives the location of the dipole as found by the inverse fit. There are 12 dots surrounding each original location, corresponding to the 12 orientations. The dots are displaced from the true location because of the presence of the image dipole (below z=0) for the forward solution but not for the inverse solution. It is dramatically evident that the inverse fits that use the Laplacian are much closer to the correct solution. For the most eccentric dipoles there is no visible error at all with the Laplacian whereas when using the raw voltages the errors are substantial. At the two smaller eccentricities the inverse solution locations for the non-Laplacian voltages are so scattered that it is not possible to tell to which dipole each solution belongs. For the Laplacian, on the other hand the clustering is still tight and the bias is still tolerably small. The finding that the error increases for the deeper dipoles is expected. As the dipoles get deeper the image dipoles causing the misspecification get closer to the electrodes. Since the strength of a dipole goes like 1/distance^2 the effect of the image dipole is a sharply increasing function of how close it is.

Note that in both figures 3a and 3b the errors are expectedly larger for the left-hand dipole which is the weaker one. Since the left dipole has half the "mass" of

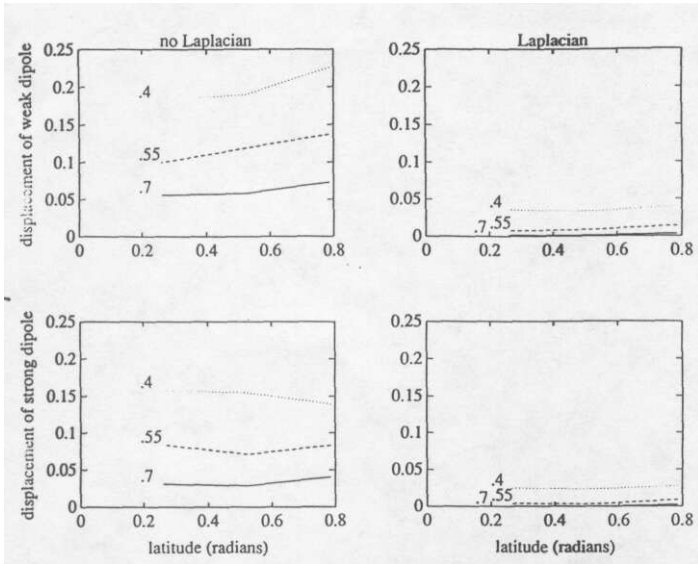

Figure 4. The data of figure 3 are replotted to provide a direct comparison between Laplacian and no Laplacian. The upper and lower panels are for the weaker and stronger dipoles. Abscissa = latitude angle, (15, 30 and 45 deg or .26, .53 and .79 radians). Ordinate = magnitude of the displacement of the inverse solution dipole location away from the original location. The three curves on each plot correspond to †he eccentricities as labeled. The discrepancy is largest for †he deepest sources since the misspecifica†ion increases with the depth of the source. The Laplacian dramatically reduces the error. As was seen in figure 3, the error is slightly less for the stronger dipole.

the right dipole it will tend to be pushed around more by the misspecification "force".

Figure 4 replots the data from figure 3 in order to provide a more quantitative picture of the effect of the Laplacian. The top pair of panels are from the weaker left-hand dipoles and the bottom pair are from the stronger member of each pair. As mentioned in the preceding paragraph the left-hand dipoles undergo a greater displacement due to model misspecification. The abscissa is the latitude angle (15, 30, or 45 deg) in radians ($\pi/12$, $2\pi/12$ and $3\pi/12$). The left and right panels show the displacement without and with the Laplacian, respectively. The displacement is the Pythagorean distance from the original dipole location (the circles in figure 3) to the location found by the nonlinear regression using the misspecified model (the dots in figure 3). Each plotted displacement value in figure 4 is the median of the 12 displacements for the 12 orientations that were calculated and shown in figure 3. The three curves in each panel correspond to the three eccentricities of the dipole pair (.7, .55 and .4), as labeled. A comparison of the right and left panels show that the errors with the Laplacian are about 10 times smaller than without the Laplacian! This is a dramatic improvement in accuracy of source localization. The Laplacian errors are negligible even in the worst case, when the sources are deep. When the two sources are at an eccentricity of .4, the error of localization is less than 4% of the radius of the sphere.

The use of a "reference electrode"

Figure 4 shows that by using the Laplacian when doing source localization the effects of misspecification are greatly reduced. The Laplacian acts by removing most of the slowly varying potentials. Normally, in a real experiment the voltages are relative to a reference electrode which is somewhat close to the active electrodes. By referring the voltages to a nearby reference we expect that the dependence on slowly varying potentials will be reduced, as it was for the Laplacian. The voltage reference for the left panels of figures 3 and 4, however, was ground rather than a nearby reference. In order to compare our results with the Laplacian to what would happen with different reference voltages we carried out a second set of simulations, similar to those done for the oblimax rotation problem. The Matlab code for these simulations is included in the Appendix (Program #2, titled *Misspec)*. One dipole was fixed to be a radial dipole on the z-axis at an eccentricity of either 0.7 or 0.5. Figure 5 is for the case in which the eccentricity of the fixed dipole is at 0.7. The right and left panels correspond to the first and second dipoles respectively, where the first dipole is the one fixed on the z-axis. The location and orientation of the second dipole was varied over a wide range of values and its magnitude was taken to be equal to that of the first dipole. The eccentricity of the second (variable) dipole had values of 0.4, 0.5, 0.6 and 0.7 (see label on each curve). The abscissa is the angular distance of the dipole from the north pole covering the range from 4.5 to 45 deg in ten steps (this was called the latitude in figure 4). For each position of the second dipole 42 orientations were chosen that were uniformly spread out on the surface of a sphere as was discussed earlier (see Function #6, *vert42* in the Appendix). The misspecified forward solution was calculated using the image dipoles as discussed earlier. The inverse solution uses the Brody formula for a one-shell spherical head. A nonlinear regression finds the positions and magnitudes of a pair of dipoles that produces the best fit to the forward solution. Details are presented in the Appendix.

Figure 5 is a plot comparing the median misspecification error using a neutral, ground reference to the error using the Laplacian. The median is taken over the 42 orientations of the magnitude of the second dipole. The results are similar to figure 4, in that the Laplacian greatly reduces the error produced by the misspecification of the inverse model. The misspecification error is not highly

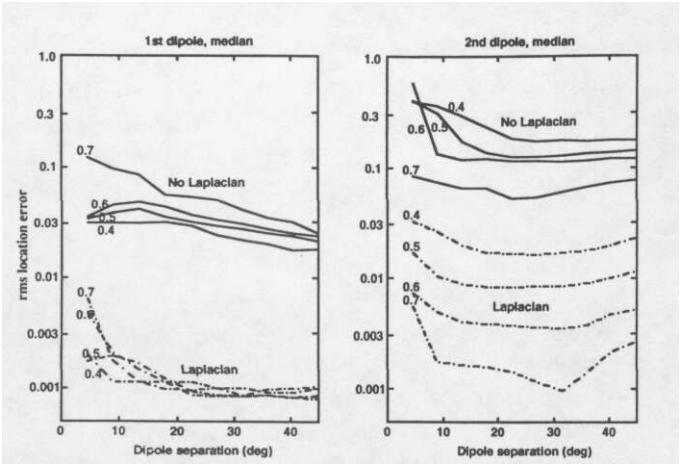

Figure 5. Data from the second simulation where the 1st dipole is a radial dipole on the z axis fixed at an eccentricity of 0.7. Abscissa = latitude of the second (variable) dipole ranging from 4.5 to 45 deg. Ordinate = median displacement of the 42 uniformly spaced orientations that were chosen for the second dipole: a value of 0.01 corresponds to 1 % of the radius of the sphere or about 1 mm. The left and right panels correspond to the fixed and the variable dipoles, respectively. With eccentricity greater than half the radius of the sphere the displacement error is 1 % with the Laplacian. Even in the worst case when the second dipole has an eccentricity of 0.4, the displacement error is still at most about 3%. The Laplacian effectively removes the contamination caused by our half-sphere model misspecification.

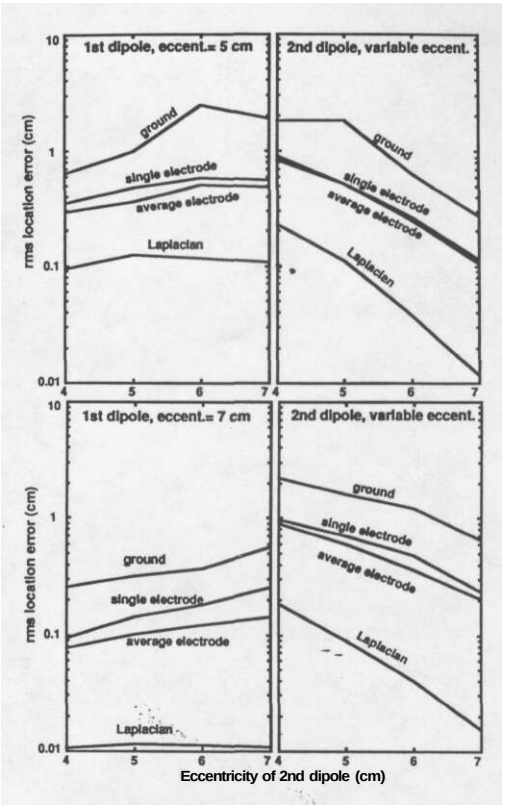

Figure 6. The rms error in location due to misspecification is plotted against the eccentricity of the second dipole. The lower two panels are for the two dipples as in figure 5. The curves labeled ground and Laplacian are obtained by averaging the corresponding data in figure 5 (No Laplacian and Laplacian) across dipole separations from 9 to 40 deg. The abscissa and ordinate are in units of cm based on assuming a head radius of 10 cm. The upper and lower panels correspond to the first (fixed) dipole being at an eccentricity of 5 and 7 cm respectively. Also shown are two active reference cases, characteristic of real data, based on a single electrode voltage and on the average voltage across all 49 electrodes. The results show that using an active reference produces an approximately three-fold reduction in rms location error as compared to the neutral, ground reference. The Laplacian produces a much larger, 10 to 20-fold improvement as compared to the neutral, ground reference. The rms location errors for dipole #l are greater in the lower than in the upper panels since a deeper dipole is more easily perturbed by the misspecification. The rms location errors for dipole #2 are similar in both upper and lower panels since location errors are not strongly dependent on the eccentricity of the other dipole.

dependent on the dipole separation (the abscissa). There is an increase in error for very close separations where the two dipoles strongly interact. There is also a gentle increase at the largest angular separations for the variable dipole because its location is nearing the boundary of the electrodes, so that the fit is less constrained.

In this second simulation we wanted to examine not only the Laplacian but also the use of an active reference as is done in real experiments. Four types of reference signal voltage were used: a) a neutral, ground reference (same as used for the left panels of figures 2-5). Use of this neutral reference gives 49 electrode voltages that are directly the voltages from the dipole sources, b) Laplacian case where there are 45 contributing electrodes since the Laplacian is not calculated at the four corner electrodes, c) an average reference whereby the average of the 49 voltages is subtracted from each. In this case there are 48 independent electrodes, d) electrode #1 is used as the reference (an arbitrary choice), and again there are 48 independent electrodes. The full computer code showing how the referencing was achieved is presented in the Appendix.

Figures 4 and 5 show that except for the very smallest separations (the abscissa) the mean square location error.. (the ordinate) is fairly independent of the angular separation of the two dipoles. This is true for all four types of referencing that we explored. Thus in figure 6 we averaged the median location errors over separations ranging from 9 to 40 deg. These averaged displacement errors of

the fit dipoles are plotted on the ordinate of figure 6. The abscissa is the eccentricity of the second dipole. In these plots units of cm are used for the abscissa and ordinate, based on assuming the head has a radius of 10 cm. The right and left panels correspond to the displacement errors of the first (fixed) and the second (variable) dipole respectively. The upper and lower panels are the results for the first dipole at an eccentricity of 0.5 and 0.7 (5 and 7 cm) respectively. The results show that the Laplacian produces a dramatic reduction in the misspecification bias across all dipole parameters examined. The displacement error is about 20 times smaller when using the Laplacian than when no active reference was used. These results are similar to those presented in figure 4. The use of a local reference produces results that are between the Laplacian and the ground reference condition. The use of the average reference produces slightly less misspecification error than when using electrode #1 as the reference. This result is reasonable since the average reference is more likely to remove the dependence on slowly varying "noise".

The ordering of the errors is as expected. Consider first the error in the variable dipole (dipole 2) as shown in the right panels of figure 6. There is a general decrease in error as the eccentricities of the dipoles increase. This is not surprising since it is expected that the misspecification error increases for deeper dipoles (the image dipole gets closer). Figure 6 also shows that the Laplacian has somewhat less benefit for deeper dipoles as would be expected since the Laplacian produces greater attenuation of deeper sources. The left panels show the complementary dependence of the first dipole's error on the second dipole's position. There is a gentle increase in error as the second dipole is more eccentric. It is expected that a more eccentric position of the second dipole produces a stronger disturbance in the location of the first dipole. The effect of the location of the second dipole on the first dipole's error is not as strong as the effect of location on its own error. A comparison between upper and lower panels reveals the same story, that a deeper dipole is more sensitive to misspecification error. Another interesting feature can be seen by examining the data when both dipoles are at the same eccentricity (5 cm in upper panels and 7 cm in lower panels). It is seen that the misspecification errors of dipole 1 is slightly smaller than that of dipole 2. That result is expected since dipole 1 is in the center of the electrode array and is thus pinned down better. The fact that dipole 1 is always radial might also help.

When doing simulations of evoked potentials it is common to use a ground reference rather than an active reference. We have shown that the use of an active reference electrode rather than a neutral reference produces a substantial improvement of the resulting fit of the source dipoles when a misspecification is present. It is somewhat surprising that the *"DC"* shift associated with the choice of reference can strongly affect the localization results. Real experiments use an active reference. Our results show that it is important to include this element of realism when doing stimulations.

An important caveat must be made about the power of the Laplacian or active reference in removing the bias due to a misspecified model. We have only tested the Laplacian for model misspecification caused by a particular shape of non spherical head. It is quite possible that the benefit of the Laplacian is less for other types of misspecification such as those produced by using a single shell model, ignoring the skull and scalp inhomogeneities. We suspect that the Laplacian's sharpening of the electrode distributions will be of benefit to a wide range of misspecifications, but further simulations are needed to answer this question.

Summary of advantages of Laplacian

The Laplacian has a number of advantages over the raw data (voltages at each electrode with a common reference): 1) The scalp potential is more localized when using the Laplacian. The separate sources stand out better and the peaks shown in the Laplacian map are closer to the true source locations than the peaks of the raw data. 2) As pointed out by Katznelson (1981) the Laplacian provides an approximation to the potential on the inner surface of the skull. Law et al. (1993) has also emphasized this advantage. 3) Baseler et al. (1994) showed that the Laplacian derivation has a higher signal-to-noise than a bipolar derivation (see discussion below).

In this article we have discussed two further advantages of using the Laplacian: 4) It improves the estimation of the rotation angle following a principal component, analysis and 5) it improves dipole source localization when a misspecified spherical model produces a bias between multiple dipoles. The first improvement would appeal to researchers who have used Laplacians in the past since the goal is to obtain a topographic map that reveals the underlying independent sources. The second improvement will appeal to researchers working on the inverse problem who are interested in using the electrode voltages to solve for the underlying current generators.

One might wonder why the Laplacian does so much better than the raw data (including use of an active reference). One could argue that the Laplacian does not contain extra information, so why should it do better in obtaining the correct oblimax rotation angle or in obtaining the correct dipole parameters. In fact the Laplacian has less information than the raw data since in order to go from the Laplacian to the raw data one needs to know

the raw voltage values on at least three extra independent electrodes (Klein 1993). So why does the Laplacian work better than the raw data? We offer three reasons:

1) The sources have less overlap in the case of the Laplacian. The decreased overlap directly reduces the bias and interactions between sources in both of the examples discussed in this paper.

2) A second argument in favor of the Laplacian for quantitative minimization problems is that it has a larger signal-to-noise ratio than the raw data. We will now present some evidence for this point since we haven't mentioned it before. Baseler et al. (1994) measured the evoked response to luminance modulated stimuli at 56 points in the visual field. Three electrodes were used with a 2 cm spacing from the middle electrode (B) to the outer electrodes (A and C). If we think of B as the reference then the two channels are: $V_A = A - B$ and $V_c = C - B$. A Laplacian channel is $V_L = -V_A - V_c = (2B - A - C)$ and a bipolar channel is $V_P = V_A - V_c = (A - C)$. Baseler et al. repeated the identical experiment on two separate days, using different m-sequence stimuli on the second day. The difference in responses between the two days provides an estimate of the noise and the sum of the two days' responses provides an estimate of the signal. By summing the square of the sum, $Sum = (Day_1 + Day_2)^2$, and difference, $Diff = (Day_1 - Day_2)^2$ responses over all 180 time bins, one obtains an estimate of the signal and noise at each electrode. The signal to noise ratio at each electrode is then given by $SNR = (Sum/Diff)^5$. Baseler et al. show histograms of the SNR both with and without the Laplacian. The Laplacian data is seen to have a preponderance of large signal-to-noise ratios in comparison to the no Laplacian data. The Laplacian derivation only responds well when the source is directly underneath the electrodes. When this happens, Baseler et al. point out that the ratio of Sum/Diff is greater than 25. This means that when the source is close to the electrodes the noise accounts for only about 4% of the variance of the signal, even though very small stimulus patches were used. More than 95% of the response is thus reproducible. One interpretation of this result is that the interfering noise has a lower spatial frequency (across the scalp) than the signal, so that the Laplacian would attenuate the noise more than it attenuates the signal. The top panel of figure 8 of Baseler et al. shows that of the 56 stimulus locations, 9 of the Laplacian derivations and zero of the non-Laplacian derivations have a Sum/Diff ratio greater than 25. If one were processing the data with linear operators the noise could be extracted at a later stage. But since both the oblimax rotation and the inverse problem dipole localization are highly nonlinear, the presence of extra noise does make a difference. It is better to rely on **the Laplacian with its reduced noise than on the noisier individual voltages V_A and V_C.**

3) The third explanation of the effectiveness of the Laplacian is that it decreases the importance of slowly varying potentials. The distortions of the scalp potential introduced by non-spherical head shapes are expected to be most severe far from the source where the potentials would be slowly varying.

After having listed so many advantages of the Laplacian, we should also list one possible disadvantage. When the signal sources are deeper than the noise sources then taking the Laplacian can decrease the signal to noise ratio. Luckily, as was just discussed (reason 2), the noise tends to have greater correlation across electrodes than does the signal and taking the Laplacian substantially increased the signal to noise ratio. However, for deep sources the Laplacian may be less useful. We can not think of other disadvantages of using the Laplacian for isolating the components and sources of evoked potentials.

Appendix: Computer programs

This Appendix contains the computer programs that were used in our simulations. There are three reasons for including these programs. First, and most important, they remove any ambiguity on how we carried out the simulations. Second, they will make it much easier for other researchers to continue with this type of work. Third, the use of the Matlab (The MathWorks, Inc.) environment makes this type of research much easier and faster than previous methods. The code in this Appendix runs equally well on UNIX, IBM and Apple computers. In the following programs we have added a line number (not part of Matlab) at the left of each line to facilitate the discussion of the programs.

Program #2: *Oblímain*

This program calculates the potential on an array of electrodes generated by two dipoles and performs an oblimax rotation on the pair. It then does another oblimax rotation on the Laplacian of the potentials.

```
%Oblimain
1  electr=electrod(15,45); Laplace=Laplac(7); dome=vert42;
2  mag(l,:)=[0 0 1]; loc(l,:)=[0 0 .7];
3   for radii = 1:4; rad = .8 -radii/10;
4    for iangsep = 1:10; angsep=pi*iangsep/40;
5   loc(2,:) = rad*[sin(angsep) 0 cos(angsep)];
6   for count = 1:42; mag(2,:) = dome(count,:);
7   data = brody(loc, mag, electr);
8  Aindiv(count,l) = abs(oblimax(data));
9  Aindiv(count,2) = abs(oblimax(data*Laplace'));
```

```
10  end;  %end of counting loop
11  Aindiv = sort(Aindiv);%the results are sorted
12  A(radii,iangsep)  = (Aindiv(21,l)+Aindiv(22,l))/2;
13 B(radii,iangsep) = (Aindiv(21,2)+Aindiv(22,2))/2;
14  end; end % end of iangsep and radii loops for second dipole
15  x=4.5*(l:10); subplot(l,2,l); plot(x, A*180/pi); subplot(l,2,2);
    plot(x, B*180/pi)
```

Line 1: The three functions *electroá, Laplac,* and *vert42* are listed and discussed later in this Appendix.

Line 2. The first dipole is defined to have unit magnitude along the z-axis [0 0 1] and to lie at an eccentricity of .7 on the z-axis [0 0 .7] (these are the calculations for the top panel of figure 2).

Line 3. The radius of the second dipole will be assigned values of .7, .6, .5, and .4.

Line 4. The angular location of the second dipole is taken to go from 4.5 to 45 deg in 10 steps.

Line 5. The second dip ole is placed on the x-z plane at the radius and angle specified by lines 3 and 4.

Line 6. The orientations of the second dipole are the vertices of a 42 vertex geodesic dome as discussed in the text (see Line 1).

Line 7. The voltages on each electrode for each dipole are calculated. The matrix *data* is a 2 x 49 matrix.

Line 8. The *oblimax* function (contained in this Appendix) is called that rotates the two vectors of electrode voltages in order to maximize the oblimax condition.

Line 9. Similar to line 8 except the oblimax operation is performed on the Laplacian of the electrode voltages. Matlab uses the convention that A' means the transpose of the matrix A.

Lines 12 and 13. The median values are stored for both the non-Laplacian (in output matrix A) and the Laplacian (in output matrix B).

Line 15. The results are plotted for the non-Laplacian (left panel) and Laplacian (right panel). The x-axis goes from 4.5 to 45 deg. Labels and titles are put on the plot afterwards.

Program #2: Misspec

This program does a two-dipole source localization for a model with a non spherical head. We have written this program so that the first part is almost identical to Program #1.

```
1  electr=electrod(15, 45); Laplace=Laplac(7); dome=vert42;
2   mag(l,l:3)=[0 0 1]; loc(l,l:3)=[0 0 .7]; inv = [1 1 -l;1 1 -1];
3   for radii=l:4; rad = .8 - radii/10;
4    for iangsep = 1:10; angsep - pi*iangsep/40;
5   loc(2,:) = rad*[sin(angsep) 0 cos(angsep)];
6   for count = 1:42; mag(2,:)=dome(count,:);
7  data = sum(brody(loc,mag, electi)+brody(loc.*inv,mag.*inv,
     electr));
8   for i_ref=l:4;% Iterate over the four types for referencing.
9     if i_ref==l, L=eye(49)-ones(49,49)/49;% average reference
10  elseif i_ref==2, L=Laplace, % Laplacian (defined in Line 1),
     local reference
11  elseif i_ref==3, L=eye(49); % eye(n) is the nxn identity
     matrix, ground reference
12  elseif i_ref==4, L(:,l)=ones(49,l); L(l,l)=0;%Use electrode 1
     as reference
13  end;
14   loc_err=leastsq('brodyinv',loc,[]],[],   electr,data*L',L)-loc;
15  Anorm(count, 2*i_ref-l:2*i_ref) = [norm(loc_err(l,:)) norm
     (loc_err(2,:))];
16  end; end; %end of counting and referencing loops
17 Asort=sort(Anorm); A_save(10*(radii-l)+iangsep)
     =(Asort(21,:) + Asort(22,:))/2;
18   end;end % end of iangsep and radii loops
19 save file_name A_save -ascii
```

Lines 1 to 6 are identical to those lines in Program #1 (except for Lines 2 and 3).

Line 2. In addition to the quantities used in Program #1, 2 x 3 matrix *inv* is defined. This will be used in line 8 to reflect the dipole across the x axis in order to obtain the image dipole.

Line 3. In Program #1, the eccentricity (rad) varied from 0.4 to 0.7. For the present simulations the eccentricity is restricted to 0.6 and 0.7 in order to simplify the plots.

Line 7. The Brody formula is used to calculate the voltage on each of the electrodes due to a pair of dipoles. The half-head voltages are generated by calling the function *brody* twice: The first time is the same as in Program #1. For the second call to *brody* the location and direction of the two dipoles are reflected around the z=0 plane so that the z position and z magnitude switches sign. Finally, the sum is taken of the voltages across each electrode so *data* is a 1 x 49 matrix. In Program #1, the summation was not taken so in that case *data* was a 2 x 49 matrix.

Lines 9 - 13. This group of lines sets up the matrix/L that is used for the four types of referencing as is indicated by the comment on each line. Consider, for example, Lines 11 and 12. Line 11 sets the L matrix to *eye* (49) which is a 49 x 49 matrix with ones on the diagonal and zeroes everywhere else. When the data vector is multiplied by this matrix it is left unchanged. Line 12 modifies this L matrix by making the first column all 1's except for the diagonal element which is set to zero. By this device when the data vector is multiplied by the L matrix the data becomes data(i)-data(l), so that electrode 1 is used as the reference electrode.

Line 14. This line calls the Metlab nonlinear (Marquardt) algorithm to minimize the difference between the half-sphere forward solution, *data,* and the regular full sphere Brody solution. The distance, *loc_err,* between the fitted dipoles and the location of the true dipoles is calculated.

Line 15. Store the location error, *loc_err,* in an array for later use. The function *norm* gives the Pythagorean sum of the distances to both displaced dipoles.

Line 17. This line calculates the median location error out of the 42 values that are calculated. The matrix Asort has 42 rows corresponding to the 42 orientations. It has 8 columns corresponding to the two dipoles for each of the four referencing conditions. The first and second dipole errors are in the odd and even columns. Since there are an even number of orientations the median is obtained by averaging two values (the 21st and 22nd).

Line 19. Store all the results for a plotting routine that is not shown.

Function #1: *Electrod*

This function defines the electrode positions by returning a (49 x 3) array of locations on a unit sphere. It is used by the Brody formula for calculating the voltages.

```
function e = electrod(step, max)
1 i = 0; % initialize the counter that specifies indexes each
    electrode.
2 for t1= -max: step: max; for t2= -max :step:max;i=i+l;
3  e(i,l) = sin(pi*tl/180)*cos(pi*t2/360);
4  e(i,2) = sin(pi*t2/180)*cos(pi*tl/360);
5 e(i,3) = sqrt(l- (e(i,l)^2) - (e(i,2)^2));
6 end; end
```

Line 2: The pair of loops are defined. Also the index i is incremented for each electrode. The argument *step* is the angle in degrees between electrodes. For all of our simulations this angle is 15 deg, so that there are 7 electrodes spanning the range from -45 to +45 deg in both the x and the y directions.

Lines 3-5. The positions are calculated as discussed in equations 8 -10 of the text.

Function #2: Oblimax

This function finds the maximum of the varimax function: $data^4/(data^2)^2$. Our own maximization routine was developed to help ensure that a local maximum would be found rather than a "more efficient" maximization routine that finds a global maximum. The present routine starts at a rotation angle of zero with a small step size of .04.

```
function ang = oblimax(data)
1 ang = -.04; step = .04; Fnew=0; % Initial search parameters
2 while abs(step) >.002 and abs(ang) <.9;
3 ang = ang+step; Fold = Fnew; % define a new angle
4 rotat = [cos(ang)  sin(ang)] * data;
5 Fnew = sum(rotat  .^4)  sum(rotat .^2).^2;
6 if Fnew <=Fold; step = -step/2.5; end
7 end % end of the while condition
```

Line 2. The search stops when the rotation angle is within .002 radians of the maximum or when it gets to be as large as .9 radian.

Line 4. This is the step that produces a rotation of the voltage distributions of the two dipoles. The variables *rotat* and *data* are 2 x 49 matrices.

Line 5. This is the varimax function discussed in the text.

Line 6. The direction of search reverses and the step size shrinks whenever the varimax function decreases.

Function #3: Brody

This function is given the locations, loc, and magnitudes, mag, of two dipoles and then calculates the voltages, *v,* on the electrode array from each of the dipoles. It gives the forward solution for a pair of dipoles in a homogeneous sphere. The voltages from the two dipoles are not added together in this function, rather they are stored in two rows of the output matrix *V.*

```
function v = brody(loc, mag, electr);
1 me= mag * electr'; md = mag * loc'; de = loc * electr';
2 h = ones(l,49); d = sqrt(l + dia*g(loc*loc')*h - 2 .* (de));
3 mdiag = me - diag(md)*h;
4 v = (me + 2 .'mdiag./(d.^2)+(de.*me -diag(md)*h)./(d+l-
    de))./d;
```

Line 1. Three-dimensional dot products are taken between the locations, magnitudes and electrode positions.

Lines 2 and 3. Two more matrices are constructed for use in Line 4.

Line 4." The Brody formula. In order to appreciate this formula one must remember that the variables *me, d, mdiag, de* and *v* are 2 x 49 matrices. The dimensions of the other quantities are: m(2,3), *electr(3,*49), *md(2,2).* Matlab achieves speed by having optimized these matrix calculations.

Function #4: *Brodyinv*

This function is a version of the Brody formula that is used in the least squares minimization routine for the inverse fit to find the best dipole parameters that match the electrode voltages stored in the vector *data.* The main difference between this function and the preceding one is that here only the dipole locations are given. This function does a least squares linear regression to find the optimal magnitude and orientation of two dipoles that best fits the forward solution data stored in *data.* A second change is that rather than outputting the electrode voltages this function outputs the difference between the calculated (inverse solution) voltages, *v,* and the forward solution voltages as required by the Matlab *leastsq* minimization routine. The dimensions of *v* are 1 x 49 whereas in the preceding function it was 2 x49

```
function v = brodyinv(loc, electr, data, L);
1 de = loc*electr'; h=ones(l,49); evolt=[];
2 d = sqrt(l + diag(loc*loc')* h - 2 .* (de));
3  for i_dipole=l:2; %this loop sums over the two dipoles
4 Ioc3 = loc(i_dipole,:)'*h; eloc3=electr'-loc3;
5  d3 = ones(3,l)*d(i_dipole,:); de3 = ones(3,l)*de(i_dipole,:);
6  F - electr'+2*eloc3 ./d3.^2 + (electr'.*de3 -Ioc3)./(d3+l-
    de3)./d3;
7 evolt = [evolt; F*L'];
8  end
9 mags = data/evolt;
10 v = mags*evolt - data + .01/(norm(diff(loc))^3+.01);
```

Lines 1 and 2. These are similar to the preceding function, the forward Brody function. In this case however, we do not

calculate *me* and *md* since the magnitudes are not given. The magnitudes will be calculated in line 9.

Lines 4-5. These two lines define the quantities that will be needed in line 6 where all quantities must have a dimension of (3,49).

Line 6. This line implements equation 13 of the text. The connection to the variables of equation 13 are: *elect* is *E,eloc3* is (E - r), *de3* is E r, and *loc3* is r.

Line 7. A 6 x 49 matrix, *evolt* is constructed by concatana ting 3 x 49 sections from each dipole. The matrix L generates the four types of referencing specified by the *mísspec* program.

Line 9. This line does the linear regression to find the magnitudes, mags. Matlab carries out the linear regression quite elegantly by using the pseudo inverse of the matrix *evolt* as discussed in the text. It should be noted that *evolt* is a 6 x 49 matrix and *mags* is a 6-dimensional vector.

Line 10. The difference between the inverse solution *mags*evolt* and the forward solution, *data,* is calculated. The final term is added to this difference in an attempt to stop the two dipoles from getting too close to each other in the least squares search. This extra "repulsion" term only becomes large when the two dipoles get very close.

Function #5. Laplac

This function generates a 49 x 49 matrix which transforms the 49 electrode voltages to the Laplacian of the voltages.

```
function L = Laplac(size)
1  L = zeros(size^2, size^2); Li = 0;
2  for x = l:size; for y = l:size
3   Li = Li+1;     % increment the counter
4   L(Li, Li) = 1; % Sets the central point of the Laplacian to unity.
5   if ((x==l I x==size)and(y==l I y==size)) L(Li, Li) - 0;
6   elseif ((x==l) I (x==size)) L(Li,[Li-l Li+1]) = -[.5 .5];
7   elseif((y==l) I (y==size)) L(Li, [Li-size Li+size]) = -[.5 .5];
8   else L(Li, [Li-size Li+size Li-1 Li+1]) = -0.25*ones(l,4);
9   end;  % End the if statement for choosing the Laplacian surround
10 end; end;  % End the two FOR loops
```

Line 1. Initialize the output matrix to have 49 rows and columns since *size* is always chosen to equal 7. Initialize *Li,* the counter for the location in the Laplacian matrix.

Line 2. Increment over the 49 electrode positions.

Line 5. For the corner electrodes do not take the Laplacian.

Line 6. Create Laplacian for the electrodes at sides x=l and x=7.

Line 7. Create Laplacian for the electrodes at sides y=l and y=7.

Line 8. Create Laplacian for the central 25 electrodes.

Function #6. vert42

This function calculates 42 points uniformly distributed on a sphere. The first twelve points are the vertices of an icosohedron at a random orientation. The remaining 30 points are at the midpoints of adjacent pairs of the first twelve points. Each point is adjusted to have unity distance from the origin.

```
function dome = vert42
1  icoso= [ 0.424936 -0.623421 -0.901522; -0.599941 0.059141 -1.009227; 0.498067 0.610145 -0.872707;  1.170388 -0.067347-0.087307; 0.487897-1.037062 0.261578;-0.606226 -0.958889 -0.308200];
2  icoso = [icoso; -icoso];                .
3  neighborl = [ 1 1 1 1 1 2 2 2   2 3 3   3 4 4 4 5 5 5 6 6 7 7 7   7 8 8  9  10 11];
4  neighbor2 = [2 3 4 5 6 3 6 10 11 4 11 12 5 8 12 8 6 9 9 10 8 9 10 11 12 9 12 10 11 12];
5  for i=l:30; midpoint(i,:)=(icoso(neighborl(i),:)+icoso(neighbor2(i),:))/ 2; end
6  icoso=icoso/sqrt(sum(icoso(l,:).^2));
7  dome=[icoso; midpoint];
```

Line 1. The three dimensional coordinates of six vertices of an icosohedron at a random orientation.

Line 2. The six vertices at the opposite side of the icosohedron are combined with the original six-to make up the twelve total vertices.

Lines 3-5. The midpoint of adjacent vertices is calculated. The original vertices were scaled so that the midpoint has unit length.

Line 6. The twelve original vertices are scaled to have unit length.

Line 7. The 42 vertices are put together.

References

Achim, A., Richer, F. and Saint-Hilaire, J. M. Methods for separating temporally overlapping sources of neuroelectric data. Brain Topography, 1988,1: 22-28.

Ary, J. P., Klein, S. A. and Fender, D. H. Location of sources of evoked scalp potentials: correction for skull and scalp thickness. IEEE Trans, on Biomed. Eng., 1981, 28: 447-452.

Baseler, H., Sutter, E. E., Klein, S. A. and Carney, T. The topography of visual evoked response properties across the visual field. Electroenceph. and Clin. Neurophys., 1994, 90: 65-81.

Brody, D. A., Terry, F. H. and Ideker, R. E. Eccentric dipole in a spherical medium: Generalized expression for surface potentials. IEEE Trans, on Biomed. Eng., 1973, BME-20: 141-143.

Darcy, T. M., Ary, J. P. and Fender, D. H. Spatio-temporal visually evoked scalp potentials in response to partial field patterned stimuli. Electroenceph. and Clin. Neurophys., 1980,50: 348-355.

Katznelson, R. D. Chapter 6 in Nunez, P. L. Electric fields of the brain: the neurophysics of EEC. New York: Oxford University Press, 1981.

Kavanagh, R. N., Darcey, T. M. and Fender, D. H. The dimensionality of the human visual evoked scalp potential. Electroenceph. and Clin. Neurophys., 1976, 40: 633-644.

Klein, S. A. Inverting a Laplacian topography map. Brain Topography, 1993,6: 79-82.

Law, S. K., Nunez, P. L. and Wijesinghe, R. S. High resolution EEC using spline generated surface Laplacians on spherical and ellipsoidal surfaces. IEEE Trans, on Biomed. Eng., 1993,40:145-153.

Maier, J., Dagnelie, G., Spekreijse, H. and Van Dijk, B. W. Principal component analysis for source localization of VEPs in man. Vision Res., 1987,27:165-177.

Mocks, J. and Verlager, R. Principal component analysis of event-related potentials: A note on misallocation of variance. Electroenceph. and Clin.Neurophys., 1986, 65: 393-398.

Mulaik, S. A. The Foundations of Factor Analysis. 1972, McGraw-Hill Book Co., New York.

Nunez, P. L. and Westdorp, A. F. The surface Laplacian, high resolution EEG and controversies. Brain Topography, 1994, 6: 221-226.

Press, W. H., Flannery, B. P., Teukolsky, S. A., and Vetterling, W. T. Numerical Recipes: The Art of Scientific Computing. 1986, Cambridge University Press, Cambridge.

Sherg, M. and von Cramon, D. A new interpretation of the generators of the BAEP waves I-V: results of a spatio-temporal dipole model. Electroenceph. and Clin. Neurophys., 1985, 62: 290-299.

Srebro, R. The Laplacian of the scalp potential field: physical interpretation and practical utility. Vision Res., 1992, 32: 257-259.

Wood, C. C. and McCarthy, G. Principal component analysis of event-related potentials: Simulation studies demonstrate misallocation of variance across components. Electroenceph. and Clin. Neurophys., 1984,59: 249-260.

van Dijk, B. W. and Spekreijse, H. The 2 dim-Laplacian field is not suitable to localize sources of EEG activity. Vision Res., 1992,32:261-262.

Zhang, Z. and Jewett, D. L. Insidious errors in dipole localization parameters at a single time-point due to model misspecification of number of shells. Electroenceph. and Clin. Neurophys., 1993,88:1-11.

Zhang, Z. and Jewett, D. L. Model misspecification detection by means of Multiple-Generator Error, using the observed potential map. Brain Topography, 1994a, 7: 29-39.

Zhang, Z. and Jewett, D. L. DSL and MUSIC under model misspecification and noise-conditions. Brain Topography, 1994b, 7:151-161.

Zhang, Z., Jewett, D. L. and Goodwill, G. Insidious errors in dipole parameters due to shell model misspecification using multiple time-points. Brain Topography, 1994, 6: 283-298.